Evaluating the Effect of the Various Directions of Seismic Input on an Irregular Building: The Former Uto City Hall

Kenji Fujii

1 Introduction

The main building of the former Uto City Hall, a five-story reinforced-concrete building damaged severely in the 2016 Kumamoto earthquakes, was an irregular building [1]. The earthquake series included a foreshock that occurred on 14 April and a main shock that occurred on 16 April 2016. In a previous study, the present author evaluated the seismic capacity of the building adopting a pushover-based procedure [2]. It was found that the seismic capacity of the building may have been insufficient to withstand the foreshock. However, this conclusion relied on the assumption that the GMRotD50 [3] (the medium of the set of geometrical means obtained using all possible rotations) spectrum represents bidirectional ground motion in a real earthquake. The effect of rupture directivity may not be negligible as the epicenter of the foreshock was not far from the target building.

The effect of the various directions of seismic input on the response of irregular (asymmetric) buildings has attracted interest from researchers (e.g., [4–6]). However, the nonlinear response makes it difficult to gain a deep understanding of the behavior. The present author considers that the mode shape changes from the initial (elastic) stage appreciably, making analysis based on the modal response complicated and difficult. Another important point for the understanding of this behavior is the energy input of each modal response: when the energy input of the first modal response were larger, some of local responses would be larger. Therefore, it is expected that the effect of the various directions of seismic input to the local response can be explained in terms of the variation of energy input of the first modal response.

K. Fujii (✉)
Department of Architecture, Chiba Institute of Technology, 2-17-1Narashino-shi Tsudanuma, Chiba 275-0016, Japan
e-mail: kenji.fujii@it-chiba.ac.jp

R. Bento et al. (eds.), *Seismic Behaviour and Design of Irregular and Complex Civil Structures IV*, Geotechnical, Geological and Earthquake Engineering 50,
https://doi.org/10.1007/978-3-030-83221-6_17

This paper reports on the nonlinear time-history analysis of the main building of the former Uto City Hall using the acceleration recorded during the foreshock, considering various directions of seismic input. Then the nonlinear first modal response is calculated from the results of nonlinear time-history analysis and pushover analysis. The following discussion focuses on (a) the relation of the variation of the peak equivalent displacement of the first modal response and the peak local responses (story drift), (b) the variation of the maximum momentary input energy [7, 8] per unit mass of the first modal response, (c) the relation of the maximum momentary input energy per unit mass of the nonlinear first modal response and the maximum momentary input energy spectrum of linear system [7–9].

2 Building and Ground Motion Data

2.1 Building Data

Figure 1 shows the simplified structural plan and elevation of the main building of the former Uto City Hall. This building was a five-story reinforced-concrete building constructed in 1965.

Damage to the building was first reported on the morning of 16 April 2016, after the main shock, even though the building experienced the foreshock on 14 April 2016. Details of the building were reported in the previous study [2].

The present nonlinear analysis uses one of the three-dimensional nonlinear frame structural models constructed in the previous study [2] (Model-RuW4-100) because this model may explain the observed structural damage of the main building of the

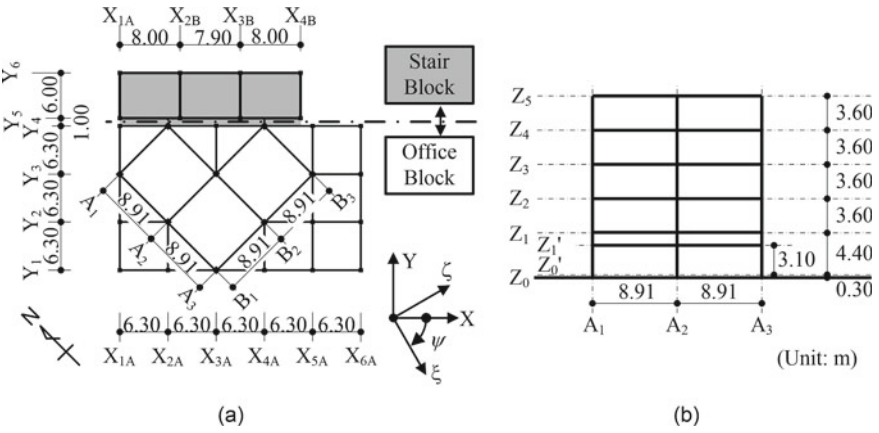

Fig. 1 Simplified structural plan and elevation of the main building of the former Uto City Hall. **a** Structural plan (level Z_0), **b** Simplified structural elevation (frame B_1)

former Uto City Hall. Figure 2 shows the structural model. As shown in Fig. 2a, this structural model is irregular in plan and elevation.

In the numerical model, a one-component model with nonlinear flexural spring at each end and the shear spring in the middle of the line element is used for all beams and columns. The concrete walls in stair block are modeled as two diagonal braces as shown in Fig. 2c, assuming that the shear behavior is predominant. Nonstructural concrete block walls are neglected in the numerical modeling, due to the lack of drawings. Other details can be found in the previous paper [2].

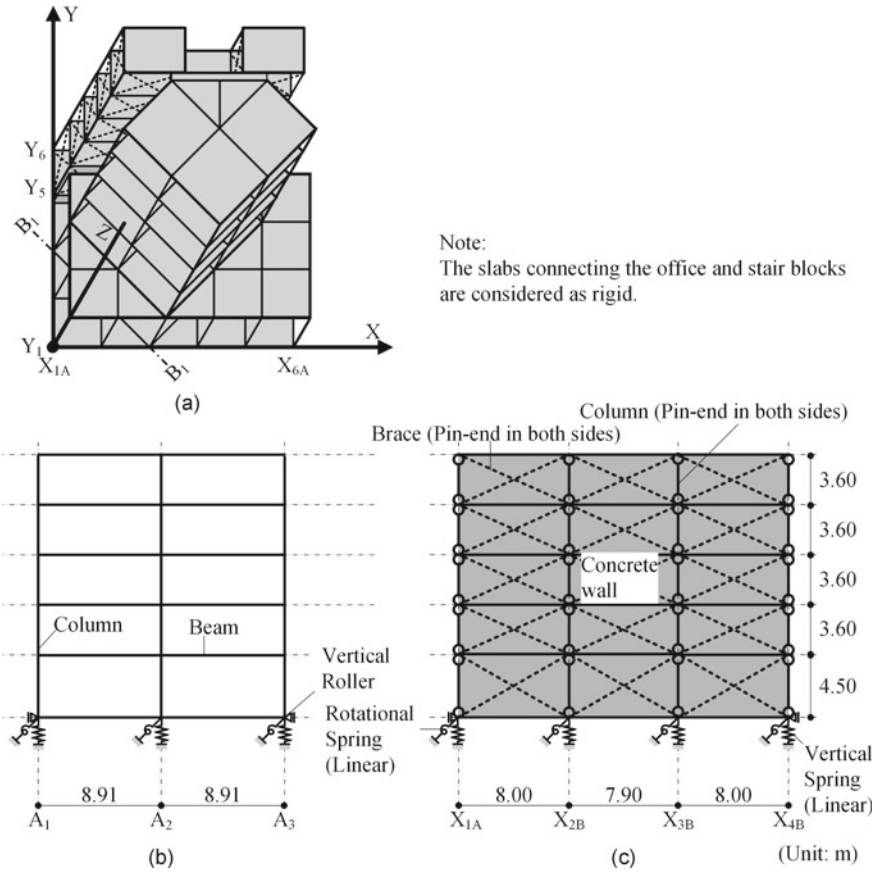

Fig. 2 Structural model [2]. **a** Overview, **b** Frame B_1, **c** Frame Y_5

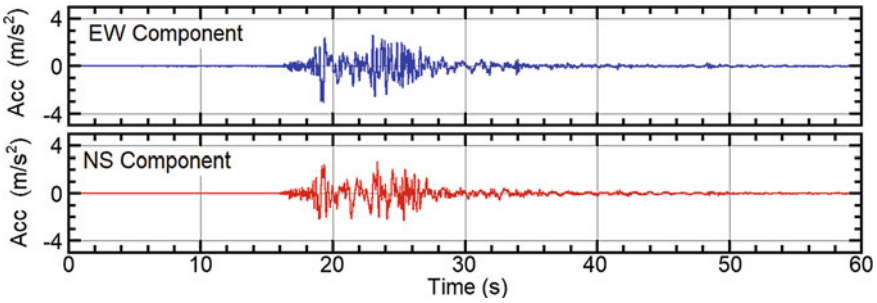

Fig. 3 EW and NS components of the foreshock acceleration recorded on 14 April at the K-NET Uto Station

2.2 Ground Motion Data

Figure 3 shows the acceleration of east–west (EW) and north–south (NS) components of the record of the foreshock (14 April 2016) obtained at the K-Net Uto Station, which is the station closest to the former Uto City Hall.

3 Nonlinear Time-History Analysis

3.1 Analysis Cases

The two components of the recorded acceleration of the foreshock are scaled by factoring constant λ ($\lambda = 0.8$, 0.9, and 1.0) in the present study. The EW and NS components are respectively input parallel to ξ- and ζ-axes, as shown in Fig. 1a. The angle of incidence of the ξ- axis with respect to the X-axis, ψ, varies at intervals 15° from 0° to 345°. Therefore, a total of $3 \times 24 = 72$ nonlinear time-history analyses are carried out. The actual EW axis is approximately 45° counterclockwise from the X-axis, and the case that $\psi = 315°$ is considered as the actual case in this study.

3.2 Analysis Results

Figure 4 shows the peak interstory drift at columns A_1B_1, A_3B_1 and A_3B_3 in the case that $\psi = 315°$. The figure also shows the drift limit assumed in the previous study [2] ($R = 1/75$). The peak responses of the "flexible" side columns (A_1B_1 and A_3B_1) are larger than the peak response of column A_3B_3, which is consistent with the fact that the observed damage to frame B_1 is more severe than that to frame A_3. In addition, the responses of columns A_1B_1 and A_3B_1 exceed $R = 1/75$ when $\lambda = 0.9$ and 1.0.

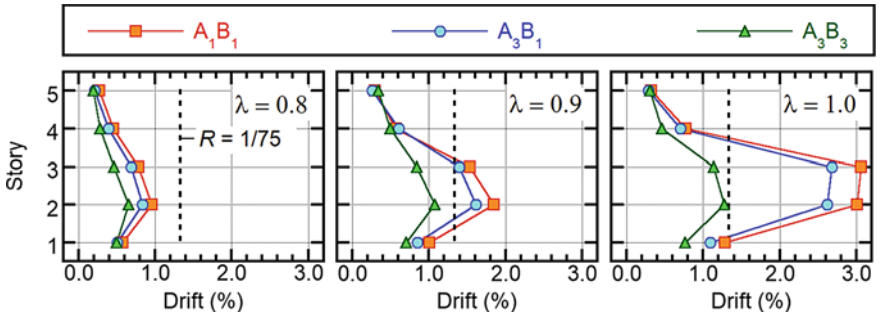

Fig. 4 Peak interstory drift at columns A_1B_1, A_3B_1 and A_3B_3 in the case that $\psi = 315°$

Figure 5 shows the distribution of the yield hinges at frame B_1. It is seen that for $\lambda = 0.9$ and 1.0, flexural yielding occurs at the top of column A_2B_1 on the third story and the right-side end of beam A_1-A_2 on level Z_3 and the left-side end of beam A_2-A_3 on level Z_3, as shown in the dotted rectangle in the figure. Note that a red triangle at a beam end indicates that the yielding of the beam–column joint occurs. Therefore, in the cases that $\lambda = 0.9$ and 1.0, the yielding of the beam–column joint and the column end occur simultaneously at the top of column A_2B_1 on the third story.

The analysis results presented here suggest that the main building of the former Uto City Hall suffered some level of structural damage during the foreshock. This finding is consistent with the results obtained in the previously conducted pushover-based evaluation [2].

Figure 6 shows the peak responses of columns A_1B_1, A_3B_1 and A_3B_3 on the second story for various directions of seismic input. As shown in plots (a) and (b),

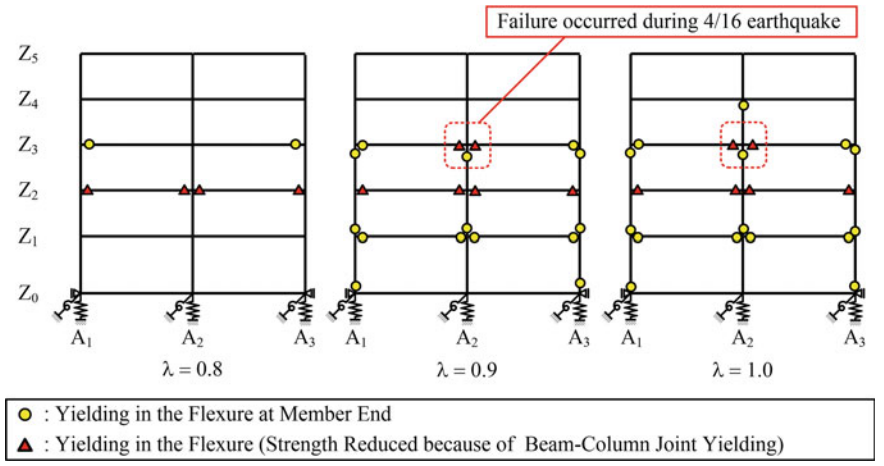

Fig. 5 Distribution of the yielding hinges at frame B_1 in the case that $\psi = 315°$

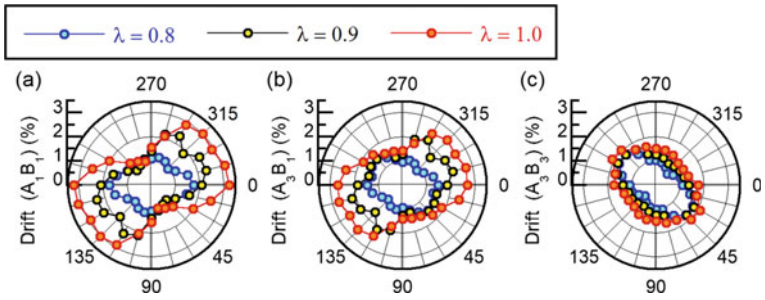

Fig. 6 Peak response at columns on the second story for various directions of seismic input. **a** Column A_1B_1, **b** Column A_3B_1, **c** Column A_3B_3

the peak responses of columns A_1B_1 and A_3B_1 are larger in the ranges of $120° \leq \psi \leq 180°$ and $300° \leq \psi \leq 360°$. In contrast, the peak response of column A_3B_3 is larger in the ranges of $0° \leq \psi \leq 75°$ and $180° \leq \psi \leq 255°$ as shown in plot (c). This implies that the damage to frame A_3 is more severe than that to frame B_1 if the direction of the seismic input is different from that of the actual earthquake.

4 Evaluation of the Effect of Various Directions of Seismic Input on the Peak Drift

4.1 Calculation of the Nonlinear First Modal Response

The nonlinear first modal response is calculated from the pushover analysis results following a procedure proposed by Kuramoto [10] for planar frame analysis.

Figure 7 compares parameters between an N-story irregular building and the equivalent single-degree-of-freedom (SDOF) model representing the first modal response [2]. Here, vectors ${}_{\mathbf{n}}\mathbf{d}$ and ${}_{\mathbf{n}}\mathbf{f}_{\mathbf{R}}$ are the displacement and restoring force vectors obtained from the pushover analysis results while $\mathbf{M}$ is the mass matrix determined from the mass and mass moment of inertia, m_j and I_j respectively, for the jth floor. Meanwhile, ${}_nD_{1U}{}^*$ and ${}_nA_{1U}{}^*$ are respectively the equivalent displacement and acceleration of the first modal response, and $M_{1U}{}^*$ is the effective first modal mass with respect to the principal axis of the first modal response (U-axis).

Figure 8 shows the flow of the calculation of the nonlinear first modal response. In this calculation, displacement-based mode-adaptive pushover (DB-MAP) analysis [2, 11] is applied to consider the change in the first mode shape at each nonlinear stage. Here, vectors $\mathbf{d}(t)$ and $\mathbf{f}_{\mathbf{R}}(t)$ are the displacement and restoring force vectors obtained from the results of nonlinear time-history analysis.

Knowing the first mode vector corresponding to ${D_{1U}}^*{}_{peak}$, $\Gamma_{1Uie}\varphi_{\mathbf{1ie}}$, the tangent of the angle of incidence of the U-axis from the X-axis, $\tan\psi_{1ie}$, is determined as.

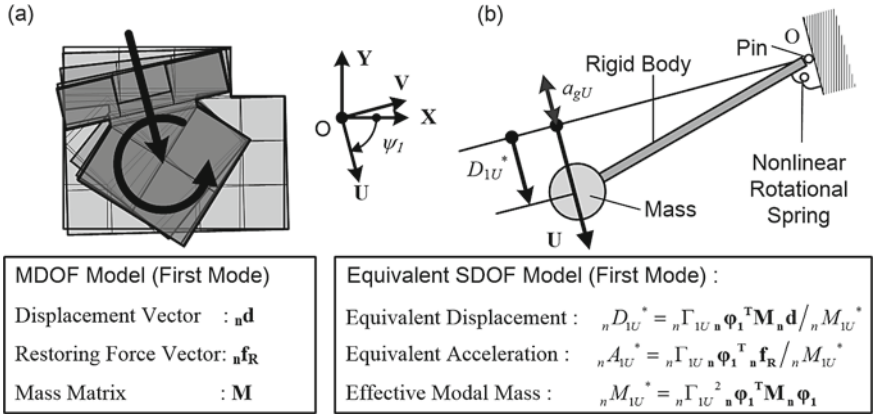

Fig. 7 Comparison of parameters between an N-story irregular building and the equivalent SDOF model. **a** An N-story irregular building with deformation similar to the first mode shape, **b** Equivalent SDOF model representing the first modal response

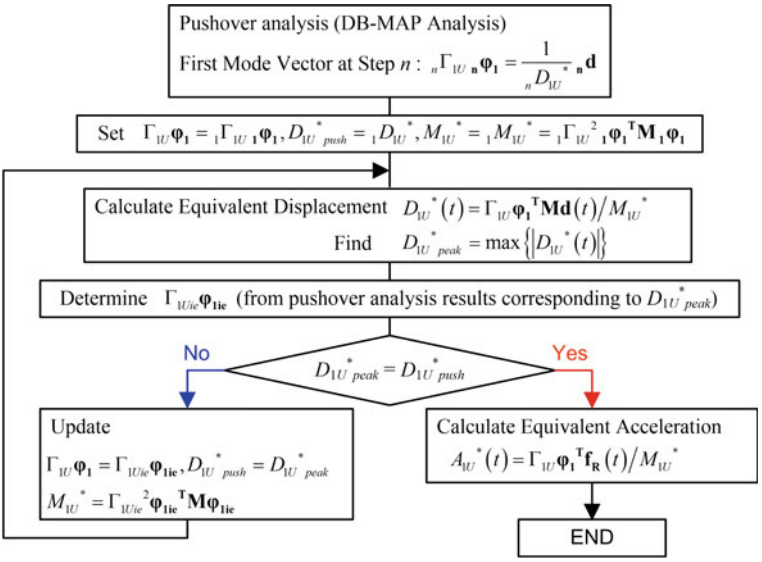

Fig. 8 Flow of the calculation of the nonlinear first modal response

$$\tan\psi_{1ie} = -\sum_j m_j\phi_{Yj1ie} \Big/ \sum_j m_j\phi_{Xj1ie} \tag{1}$$

$$\varphi_{\mathbf{1ie}} = \left\{ \phi_{X11ie}\cdots\phi_{XN1ie}\ \ \phi_{Y11ie}\cdots\phi_{YN1ie}\ \ \phi_{\Theta 11ie}\cdots\phi_{\Theta N1ie} \right\}^{\mathbf{T}}. \tag{2}$$

4.2 *Effect of Various Directions of Seismic Input on the Nonlinear First Modal Response*

Figure 9 shows the results of calculating the peak of the first modal response ($D_{1U}{}^{*}{}_{peak}$ and $A_{1U}{}^{*}{}_{peak}$) from all results of time-history analysis. Plot (a) compares the peak of the first modal response and $A_{1U}{}^{*} - D_{1U}{}^{*}$ relationship obtained from the pushover (DB-MAP) analysis. Those peaks of the nonlinear first modal response fairly agree to $A_{1U}{}^{*} - D_{1U}{}^{*}$ relationship obtained from the pushover analysis. This confirms that the nonlinear first modal response is properly calculated by the procedure presented herein. Plot (b) shows the peak equivalent displacement $D_{1U}{}^{*}{}_{peak}$ for various directions of seismic input. As shown in plot (b), $D_{1U}{}^{*}{}_{peak}$ is larger in the ranges of $120° \leq \psi \leq 180°$ and $300° \leq \psi \leq 360°$.

A comparison of Figs. 9b and 6 shows that the range in which $D_{1U}{}^{*}{}_{peak}$ is largest corresponds to the range in which the peak responses of columns A_1B_1 and A_3B_1 are largest, while this is not so for column A_3B_3.

Figure 10 shows the relation of the peak equivalent displacement of the first modal response and the peak drift of the columns on the second story. The figure

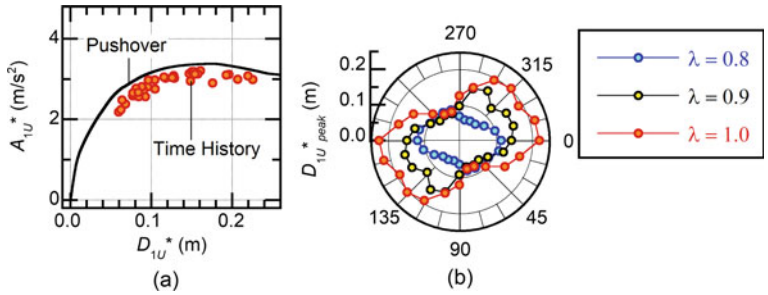

Fig. 9 Calculation results of the peak of the first modal response. **a** Equivalent acceleration-equivalent displacement ($A_{1U}{}^{*} - D_{1U}{}^{*}$) relationship, **b** $D_{1U}{}^{*}{}_{peak}$ for various directions of seismic input

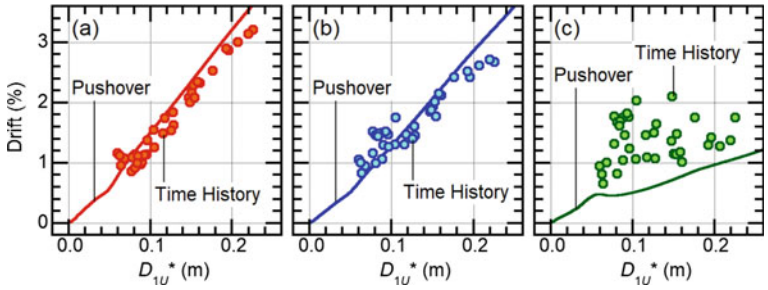

Fig. 10 Relation of $D_{1U}{}^{*}{}_{peak}$ and the peak drift of columns on the second story. **a** Column A_1B_1, **b** Column A_3B_1, **c** Column A_3B_3

compares the results of nonlinear time-history analysis and pushover analysis. For columns A_1B_1 and A_3B_1, the results of nonlinear time-history analysis agree well with the results of pushover analysis, as shown in Fig. 10a, b. In contrast, there is an appreciable difference between the results of nonlinear time-history analysis and pushover analysis for column A_3B_3 as shown in Fig. 10c.

From this observation, the drift responses of columns A_1B_1 and A_3B_1 on the second story can be approximated using the first modal response, while the contributions of the second and higher modal responses are appreciable for column A_3B_3. The variation in the peak drift on the second story at the "flexible" side columns (A_1B_1 and A_3B_1) due to the direction of the seismic input can therefore be explained in terms of the variation of the first modal response.

4.3 *Momentary Energy Input of the Nonlinear First Modal Response*

The momentary input energy of the first modal response per unit mass is next calculated. The present study follows studies by Inoue and coauthors [7, 8]. The energy input during a half cycle of the structural response is considered. The momentary input energy of the first modal response per unit mass, $\Delta E_{1U}{}^*/M_{1U}{}^*$, is defined as.

$$\frac{\Delta E^*_{1U}}{M^*_{1U}} = -\int_t^{t+\Delta t} a_{gU}(t)\dot{D}^*_{1U}(t)dt \tag{3}$$

where $a_{gU}(t)$ is the ground acceleration component along the U-axis while t and $t + \Delta t$ are the beginning and end times of a half cycle of the structural response. The maximum momentary input energy of the first modal response per unit mass, $\Delta E_{1U}{}^*{}_{\max}/M_{1U}{}^*$, is defined as the maximum value of $\Delta E_{1U}{}^*/M_{1U}{}^*$ over the course of the seismic event.

Figure 11 illustrates the definition of $\Delta E_{1U}{}^*{}_{\max}/M_{1U}{}^*$. In the figure, the case in which the largest $D_{1U}{}^*{}_{peak}$ occurs ($\lambda = 1.0$, $\psi = 0°$) is shown as an example. As shown in the figure, $\Delta E_{1U}{}^*{}_{\max}/M_{1U}{}^*$ is the input energy from $t = 24.34$ s (beginning of a half cycle as shown in (a)) to $t + \Delta t = 25.06$ s (end of the half cycle).

For the following discussions, the equivalent velocity of the maximum momentary input energy of the first modal response, $V_{\Delta E1U}{}^*$, is defined as.

$$V_{\Delta E1U^*} = \sqrt{2\Delta E_{1U^*}\max/M_{1U^*}} \tag{4}$$

Figure 12 shows the results of calculating $D_{1U}{}^*{}_{peak}$ and $V_{\Delta E1U}{}^*$ from all results of time-history analysis. Plot (a) shows a clear relation between $D_{1U}{}^*{}_{peak}$ and $V_{\Delta E1U}{}^*$, as was pointed out by Inoue and coauthors for the nonlinear SDOF model [7, 8]. Plot (b) shows the peak equivalent velocity $V_{\Delta E1U}{}^*$ for various directions of seismic input.

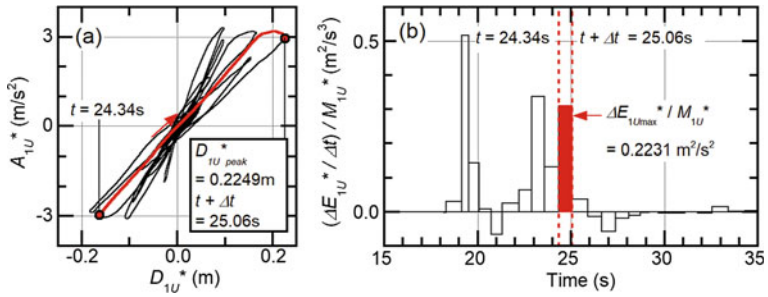

Fig. 11 Definition of the maximum momentary input energy of the first modal response per unit mass. **a** Hysteresis loop of the first modal response, **b** Time-history of the momentary energy input

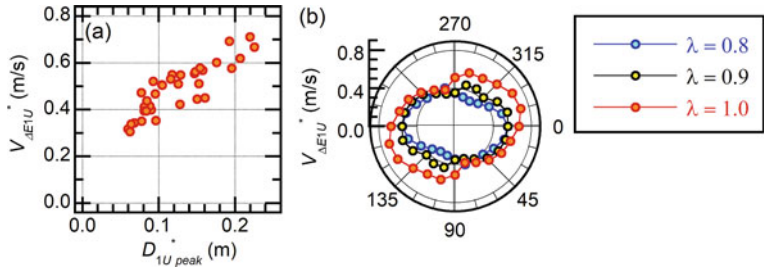

Fig. 12 Calculation results of $D_{1U}{}^{*}{}_{peak}$ and $V_{\Delta E1U}{}^{*}$. **a** Relation of $D_{1U}{}^{*}{}_{peak}$ and $V_{\Delta E1U}{}^{*}$, **b** $V_{\Delta E1U}{}^{*}$ for various directions of seismic input

As shown in plot (b), $V_{\Delta E1U}{}^{*}$ is larger in the ranges of $135° \leq \psi \leq 180°$ and $315° \leq \psi \leq 360°$. The trend of $V_{\Delta E1U}{}^{*}$ is consistent to that of $D_{1U}{}^{*}{}_{peak}$ shown in Fig. 9b. Therefore, the variation in the peak drift on the second story at the "flexible" side columns (A_1B_1 and A_3B_1) due to the direction of the seismic input can be explained in terms of the variation of $V_{\Delta E1U}{}^{*}$.

4.4 Comparison of the Maximum Momentary Input Energy with the Linear Spectrum

Next, the maximum momentary input energy of the first modal response shown above is compared with the linear spectrum. In this study, the following linear spectra are calculated: (i) the maximum and minimum linear unidirectional $V_{\Delta E}$ spectra with viscous damping ratio $h = 0.10$ [7, 8] considering various angle of incidence of seismic input, and (ii) linear bidirectional $V_{\Delta E}$ spectrum [9] with viscous damping ratio $h = 0.10$. Since the angle of incidence of the U-axis from the X-axis varies gradually as the equivalent displacement $D_{1U}{}^{*}{}_{peak}$ increases due to the nonlinearity, the intervals for calculating the maximum and minimum $V_{\Delta E}$ spectrum should be

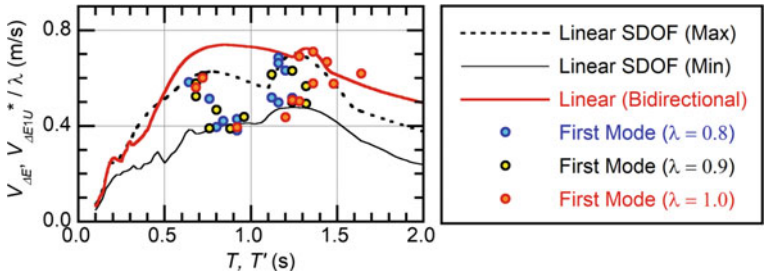

Fig. 13 Comparisons of the normalized $V_{\Delta E1U}{}^{*}$ and linear $V_{\Delta E}$ spectrum

smaller. Therefore, the maximum and minimum $V_{\Delta E}$ spectrum is calculated for a for a natural period of the linear SDOF model T when the angle of incidence of the seismic input ψ varies in 1° intervals from 0° to 359°. Figure 13 compares the $V_{\Delta E1U}{}^{*}$ normalized by the scaling factor λ and linear $V_{\Delta E}$ spectrum with viscous damping ratio $h = 0.10$. In the figure, the notations Max and Min respectively indicate the maximum and minimum $V_{\Delta E}$, while the notation Bidirectional is the bidirectional momentary input energy spectrum calculated using time-varying function [9]. The response period T' is defined from the time for a half cycle of the structural response at $\Delta E_{1U}{}^{*}{}_{\max}/M_{1U}{}^{*}$ as.

$$T' = 2\Delta t \tag{5}$$

In the figure, most plots of the normalized $V_{\Delta E1U}{}^{*}$ are within the band between Max and Min $V_{\Delta E}$ spectra. In addition, the bidirectional $V_{\Delta E}$ spectrum approximates the upper bound of the plots of the normalized $V_{\Delta E1U}{}^{*}$. Therefore, for the conservative prediction of the peak response, the bidirectional $V_{\Delta E}$ spectrum formulated in [9] may be used as the seismic intensity parameter.

5 Conclusions

A nonlinear time-history analysis of the main building of the former Uto City Hall was carried out, considering various directions of seismic input. The effect of various directions of seismic input on the peak response was then discussed based on the nonlinear first modal response. The main conclusions of the study are as follows.

(a) The angle of incidence where the peak drift at the "flexible" side column (A_1B_1 and A_3B_1) is the largest is close to that where the peak equivalent displacement of the first mode, $D_{1U}{}^{*}{}_{peak}$, is largest.

(b) The equivalent velocity of the maximum momentary input energy of the first modal response, $V_{\Delta E1U}{}^{*}$, is clearly related to $D_{1U}{}^{*}{}_{peak}$. This is consistent to

the results by Inoue and coauthors for the nonlinear SDOF model. In addition, the trend of the variation of $V_{\Delta E1U}{}^{*}$ is consistent to that of $D_{1U}{}^{*}{}_{peak}$.

(c) Most plots of the evaluated $V_{\Delta E1U}{}^{*}$ are within the band between the maximum and minimum spectra obtained from the linear elastic analysis considering all possible angles of incidence. In addition, the bidirectional $V_{\Delta E}$ spectrum formulated in [9] approximates the upper bound of $V_{\Delta E1U}{}^{*}$.

Based on these findings, the presenting author considers the effect of the various directions of seismic input to the local response at "flexible" side can be explained in terms of the variation of energy input of the first modal response. In addition, the equivalent velocity of the bidirectional maximum momentary input energy may be one of the possible seismic intensity parameters available for discussion of the nonlinear peak response under bidirectional excitation. Further investigation is needed for confirmation.

Acknowledgements Ground motions used in this study were taken from the websites of the National Research Institute for Earth Science and Disaster Resilience (NIED) (http://www.kyoshin.bosai.go.jp/kyoshin/, last accessed on 14 December 2019).

References

1. Fujii K, Yoshida S, Nishimura T, Furuta T (2017) Observations of damage to Uto City Hall suffered in the 2016 Kumamoto Earthquake. In: Proceedings of the 8th European workshop on the seismic behaviour of irregular and complex structures, Bucharest, Romania
2. Fujii K (2019) Pushover-based seismic capacity evaluation of Uto City Hall damaged by the 2016 Kumamoto Earthquake. Buildings 9(6):140. https://doi.org/10.3390/buildings9060140
3. Boore DM, Watson-Lamprey J, Abrahamson NA (2007) Orientation-independent measures of ground motion. Bull Seismol Soc Am 96:1502–1511
4. López OA, Torres R (1997) The critical angle of seismic incidence and the maximum structural response. Earthq Eng Struct Dynam 26:881–894
5. Athanatopoulou AM (2005) Critical orientation of three correlated seismic components. Eng Struct 27:301–312
6. Faggella M, Gigliotti R, Mezzacapo G, Spacone E (2018) Graphic dynamic prediction of polarized earthquake incidence response for plan-irregular single story buildings. Bull Earthq Eng 16(10):4971–5001
7. Inoue N, Wenliuhan H, Kanno H, Hori N, Ogawa J (2000) Shaking table tests of reinforced concrete columns subjected to simulated input motions with different time durations. In: 12th World conference on earthquake engineering. Auckland, New Zealand
8. Hori N, Inoue N (2002) Damaging properties of ground motion and prediction of maximum response of structures based on momentary energy input. Earthq Eng Struct Dynam 31(9):1657–1679
9. Fujii K, Yoshiki Murakami Y (2020) Bidirectional momentary energy input to a one-mass two-DOF system. In: Proceedings of the 17th world conference on earthquake engineering. Sendai, Japan

10. Kuramoto H (2004) Earthquake response characteristics of equivalent SDOF system reduced from multi-story buildings and prediction of higher mode responses. J Struct Construct Eng. Trans AIJ 580:61–68 (in Japanese)
11. Fujii K (2014) Prediction of the largest peak nonlinear seismic response of asymmetric buildings under bi-directional excitation using pushover analyses. Bull Earthq Eng 12:909–938